




Numerical study on three-stage ignition of dimethyl ether by hot air under engine-relevant conditions

Xinyi Chen^a, Zisen Li^a, Yiqing Wang^a, Wang Han^b, Arne Scholtissek^b, Peng Dai^c,
Christian Hasse ^b and Zheng Chen^{a*}

^aSKLTCS, CAPT, BIC-ESAT, Department of Mechanics and Engineering Science, College of Engineering, Peking University, Beijing, People's Republic of China; ^bInstitute for Simulation of reactive Thermo-Fluid Systems, TU Darmstadt, Darmstadt, Germany; ^cDepartment of Mechanics and Aerospace Engineering, Southern University of Science and Technology, Shenzhen, People's Republic of China

(Received 10 May 2023; accepted 16 September 2023)

Non-premixed combustion often occurs in practical engines, and it is affected by the coupling effects of chemical kinetics and transport. This study aims to elucidate the individual effect of chemical kinetics, molecular diffusion, and convective transport on non-premixed combustion. To this end, three types of reactive systems are investigated by numerical simulations considering detailed chemistry and transport: (1) thermochemical system: 0D homogeneous autoignition, (2) thermochemical-diffusive system: 1D non-premixed ignition in a static diffusion layer, (3) thermochemical-diffusive-convective system: 1D non-premixed ignition in a counterflow and 2D lifted flame in a coflow. The simulations are carried out for diluted dimethyl ether and hot air under engine-relevant conditions with a pressure of 40 atm and hot air temperatures of 700 ~ 1500 K. First, homogeneous ignition process of DME/air premixture is investigated. It is found that, apart from the low- and high-temperature chemistry which are essential in the typical two-stage ignition, the intermediate-temperature chemistry can also play an important role, especially for slow reaction process in fuel rich regions. Then, the effects of thermochemical conditions and molecular diffusion are assessed for non-premixed ignition process in the 1D diffusion layer. The results show that, the reaction front always initiates from local autoignition in most reactive regions; then it propagates either in sequential auto-ignition mode or in diffusion-driven mode as a deflagration wave. With various thermochemical conditions, the chemical kinetics behave differently and produce complex multibrachial (tetrabrachial, pentabrachial and hexabrachial) structures during the reaction front propagation. Decreasing the diffusion layer thickness generally delays the reaction front initiation but enhances its transition into a diffusion-driven flame. Finally, it is shown that 1D diffusion layer simulations can qualitatively reproduce the complex multibrachial structures in 1D counterflow and 2D coflow at certain conditions. A regime diagram is proposed to separate the effects of chemical kinetics, molecular diffusion, and convective transport.

Keywords: non-premixed combustion; dimethyl ether; three-stage ignition; intermediate-temperature chemistry

*Corresponding author. Email: cz@pku.edu.cn

1. Introduction

Non-premixed combustion is widely used in many practical combustion facilities, such as diesel engines [1], multi-staged combustors and afterburners [2]. In these facilities, fresh fuel is injected into a high-temperature environment at a high speed and then mixes with hot oxidiser in a diffusion layer. After successful ignition, a non-premixed flame is established in the cylinder. The structure and stabilisation mechanisms of the non-premixed flame have great impact on both fuel efficiency and pollutant formation [1]. Therefore, understanding the non-premixed combustion process in these devices is extremely important for engine design.

Generally, two configurations have been extensively used to study the non-premixed convective-diffusive systems: one is the strained counterflow configuration with opposing streams of fuel and oxidiser, and the other is the coflow configuration with separating free streams of fuel and oxidiser. In the counterflow configuration, the mixing of fuel and oxidiser strongly depends on the flow velocity gradient or strain rate. Therefore, the non-premixed ignition process is governed by both transport and chemical kinetics. This is characterised by the S-curve response of maximum temperature to the strain rate [3] and heated oxidiser temperature [4]. Recently, Zheng et al. [5] and Deng et al. [4] have investigated the ignition of dimethyl ether (DME) by hot air in counterflow and addressed the importance of low-temperature kinetics in the non-premixed ignition process of large hydrocarbons.

On the other hand, in the coflow configurations the flow velocity is normal to the composition gradient and the transverse mixing. Nevertheless, convective transport and chemical kinetics are still essential to the structure and stabilisation mechanism in lifted flames. In the literature, tremendous effort [6–10] has been devoted to understanding the structure and stabilisation mechanism of the lifted flames. At non-autoignitive conditions, the edge flame is always stabilised by the dynamic balance between the inlet flow and local flame propagation [7]. As discussed by Buckmaster [6], the edge flame often consists of a lean and rich premixed flame wing with a trailing non-premixed flame centred at the stoichiometric mixture fraction, appearing as a classical triple flame. However, in real engines, the mixture is exposed to an elevated temperature and pressure environment, where autoignition can be activated and then interact with the edge flame. In order to understand the stabilisation mechanism at autoignitive conditions, Chung and his co-workers [11, 12] experimentally studied the non-premixed methane and propane jet flames. They found that the lifted flames can also be stabilised by autoignition. More recently, Krisman et al. [8] and Deng et al. [9, 13] have conducted a series of 2D simulations for DME/air coflow flames under engine relevant conditions. They found that with the presence of low temperature chemistry, the edge flame could translate into a tetrabrachial or pentabrachial structure at high oxidiser temperatures. Furthermore, they found that the lifted flame could be stabilised by kinematics, chemical kinetics, or a combination of both depending on the boundary temperature and stream inlet velocity. Except to the streamwise transport, the transverse molecular mixing was also shown to have a large impact on the lifted flame structure and stabilisation mechanism by Dalakoti and his co-workers [14].

The above studies demonstrated that chemical kinetics, molecular diffusion as well as convective transport play a crucial role in the non-premixed combustion. However, in previous 2D flow configurations, these three effects co-exist and are always coupled. It is still unclear how they individually affect the non-premixed combustion. Therefore, the objective of present study is to perform a systematic analysis to elucidate the individual effects of

chemical kinetics, molecular diffusion, and convective transport on laminar non-premixed combustion processes. To this end, three types of reactive systems are considered here. The first one is the 0D autoignition process, for which the local premixture is sampled from an established diffusion layer. With the absence of molecular diffusion and convective transport, the autoignition kinetics can be isolated and analyzed. The second one is non-premixed ignition process in an initially static 1D diffusion layer, in which the effects of molecular diffusion can be examined. The third type includes the 1D counterflow and 2D lifted flame in a hot coflow, both of which are affected by forced convective transport.

This paper is organised as follows. In Section 2, the fuel considered here is introduced, and the models and numerical methods are presented. Section 3 considers the three-stage ignition process in a 0D homogeneous system, which is followed by the non-premixed ignition in a 1D diffusion layer considered in Section 4. In Section 5, the non-premixed combustion in counterflow and coflow with forced convective transport is studied. Section 6 compares the results for different configurations and discusses the effects of chemical kinetics, molecular diffusion, and convective transport. Finally, the concluding remarks are given in Section 7.

2. Models and numerical methods

DME is selected as the target fuel in present study. Compared to conventional diesel fuels, use of DME in engines can lead to a reduction in soot and NO_x formation due to its special structure [15] and hence DME has been proposed as a future transportation fuel. Previous studies have shown that DME can undergo either a single- or two-stage ignition process depending on the initial mixture temperature, pressure and radical concentration [16]. Typically, the explosion mode of low-temperature chemistry (LTC) is argued to be associated with the decomposition of $\text{O}_2\text{CH}_2\text{OCH}_2\text{O}_2\text{H}$, which results in the formation of two OH molecules and highly oxygenated intermediates, e.g. $\text{HO}_2\text{CH}_2\text{OCHO}$ and OCH_2OCHO . With the presence of LTC, the mixture temperature would rise mildly by a low-temperature heat release, which is accordingly termed as the first-stage ignition. The second rapid fuel oxidation period is mainly governed by high-temperature chemistry (HTC). It is featured by CO oxidation reactions and the chain branching reaction $\text{H} + \text{O}_2 = \text{O} + \text{OH}$. Between these two ignition stages, there is a period within an intermediate-temperature regime which often receives less attention. Generally, the chemical pathway in this intermediate-temperature regime is argued to be correlated with the chain-branching reaction of hydrogen-peroxide (H_2O_2) decomposition [17]. However, under most thermochemical conditions, the intermediate-temperature heat release was not considered as a distinct stage of ignition since H_2O_2 decomposition quickly translates to $\text{H} + \text{O}_2$ chain branching and the intermediate-temperature heat release quickly merges with the high-temperature heat release [18]. Recently, the intermediate-temperature heat release has been found to behave as a single ignition stage during the ignition process of DME/air [19], *n*-heptane/air [18, 20], diethyl ether/air as well as diethyl ether/ethanol/air blend mixtures [21], and multi-stage ignition behaviour was observed for these mixtures. Furthermore, the dynamics of non-premixed and premixed cool flames, warm flames and hot flames has been widely investigated in the literature [22]. In this work, the importance of intermediate-temperature chemistry (ITC) is further highlighted in non-premixed combustion. The emphasis is placed on the transition between LTC/ITC/HTC dominated ignition, cool flame, warm flame, and hot flame in an auto-igniting mixture relevant to

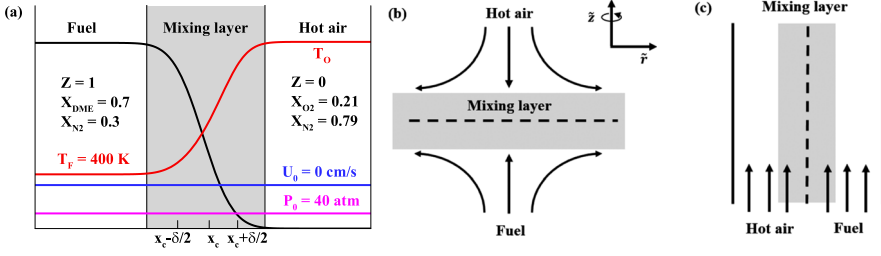


Figure 1. Schematics of (a) 1D diffusion layer, (b) 1D axisymmetric counterflow and (c) 2D planar coflow. x_c denotes the centre of the diffusion layer and δ is the diffusion layer thickness (colour online).

engine conditions. In all simulations, the chemical kinetics of DME is modelled by the skeletal mechanism of 39 species and 175 elementary reactions, which was reduced from the detailed mechanism of Zhao et al. [23] by Bhagatwala et al. [24]. As shown in the Supplementary document, the same multistage ignition results are predicted by the skeletal and detailed mechanisms. Therefore, the skeletal mechanism is used here to reduce the computational cost.

Besides the 0D autoignition process, the non-premixed ignition and flame in three configurations depicted in Figure 1 are considered. The corresponding numerical models are presented and discussed in the following.

2.1. Non-premixed ignition in a 1D diffusion layer

To examine the effects of molecular diffusion on non-premixed autoignition, we consider the transient ignition process in a 1D planar diffusion layer [2]. As shown in Figure 1(a), the computational domain is $0 \leq x \leq 2 \text{ cm}$. The left side of the domain is the cold fuel, which consists of 70% DME and 30% N_2 (by volume percentage) at an initial temperature of $T_F = 400 \text{ K}$. The right side is the hot air at a higher temperature of T_O ranging from 700 to 1500 K. The composition is characterised by the mixture fraction, Z , which measures the local element fractions that emanates from the fuel stream. In the current work, the Bilger mixture fraction is used [25, 26]:

$$Z = \frac{\frac{2Y_C}{W_C} + \frac{Y_H}{2W_H} + \frac{Y_{O,O}-Y_O}{W_O}}{\frac{2Y_{C,F}}{W_C} + \frac{Y_{H,F}}{2W_H} + \frac{Y_{O,F}}{W_O}} \quad (1)$$

where Y_k denotes the mass fraction of k -th element and $Y_{k,F}$, $Y_{k,O}$ refer to mass fraction of k -th element in fuel and oxidiser stream, respectively. The initial mixture fraction distribution in the diffusion layer is specified by [2]:

$$Z = \frac{1}{2} \left[1 - \text{erf} \left(\frac{x - x_c}{\delta} \right) \right] \quad (2)$$

where erf is an error function, x_c denotes the centre of the diffusion layer and δ characterises the diffusion layer thickness. Three different values of thickness $\delta = 10, 100, 1000 \mu\text{m}$ are selected to investigate the effect of molecular diffusion on the ignition, and x_c is fixed to be 0.6 cm in all simulations. The distribution of Y_k and the enthalpy h in the diffusion layer can be initialised assuming a linear mixing form between the fuel and oxidiser

streams:

$$Y_k = Z \cdot Y_{k,F} + (1 - Z) \cdot Y_{k,O} \quad (3)$$

$$h = Z \cdot h_F + (1 - Z) \cdot h_O \quad (4)$$

In the above equations, $Y_{k,F}$ and $Y_{k,O}$ denote the mass fractions of k -th species on fuel and oxidiser side and h_F and h_O denote the enthalpy of the cold fuel and hot air, respectively. The initial temperature is determined according to the local enthalpy and composition. The flow field is initially static (i.e. $U_0 = 0$ cm/s) with a pressure of $P_0 = 40$ atm. Outlet boundary conditions that enforce zero gradients of mass fractions and temperature are used at $x = 0$ and 2 cm.

The transient simulation of ignition process is conducted using the in-house code A-SURF [27–29]. A-SURF solves the reactive multispecies Navier-Stokes equations in conservative form with the finite volume method. It has been successfully used in previous studies [30–34] on both premixed and non-premixed ignition problems. Details of the governing equations and numerical schemes are presented in Refs [27–29]. Adaptive mesh refinement is used to resolve the fine flame structures within the mixing layer. The finest level mesh size is $1.5 \mu\text{m}$ for cases with $\delta = 1000$ and $0.75 \mu\text{m}$ for cases with $\delta = 100$ and $10 \mu\text{m}$ respectively, which was demonstrated to yield accurate and mesh-independent results by grid convergence tests.

2.2. Non-premixed ignition in 1D counterflow

To identify the impact of convective transport on the autoignition of DME, the transient ignition process in a 1D axisymmetric laminar counterflow shown in Figure 1(b) is simulated. The flow configuration is initialised by a cold N_2 -diluted fuel stream (70% DME and 30% N_2 by volume percentage) with $T_F = 400$ K against a hot air stream with a higher temperature of T_O . At first, all the chemical source terms are set to zero until the non-reacting flow reached the steady state. The frozen flow constraint is used to determine the initial composition and temperature profiles within the diffusion layer. The chemical reactions are then activated; the mixture autoignites and the subsequent evolution of reaction front is simulated. By selecting different values of inlet velocity (i.e. V_F and V_O) and the distance between the two opposed inlets (i.e. L), the strain rate of initial frozen flow a is varied. For the present study, strain rate values of $a = 310$ and 886 1/s are selected, which yield initial diffusion layer thickness of $\delta \sim 1000$ and $10 \mu\text{m}$, respectively. In this study, the transient counterflow calculations are conducted by an in-house solver ULF [35, 36].

2.3. Stabilised lifted flame in 2D coflow

We also consider a convective mixing layer in a 2D rectangular computational domain, as shown in Figure 1(c). The flow configuration is a cold fuel stream with a heated coflow of air. The inlet condition is a convective mixing layer, the composition and temperature profiles of which are specified by the same equations, Equations (2–4), as that in 1D diffusion layer. To study the potential effect of scalar dissipation rate on the flame structure, the parameter δ in Equation (2) is varied to give different mixing layer thickness. For the present study, values with $\delta = 10, 1000 \mu\text{m}$ are selected. The 2D computational domain is in a size of $5 \text{ mm} \times 1.5 \text{ mm}$ or $5 \text{ mm} \times 10 \text{ mm}$ in the y (streamwise) and z (transverse) direction, depending on the case. Uniform grid spacing in the streamwise direction is set to

$\Delta y = 5 \mu\text{m}$ and non-uniform grid with minimum $\Delta z = 0.75 \mu\text{m}$ is set in the transverse direction to resolve the mixing layer. At the inlet, uniform velocities of 10 m/s for both streams are specified, which minimises the effect of shear on flame structure. The burned mixture leaves the domain from the outlet, where zero gradients of velocity, temperature and mass fractions are enforced. The lateral boundaries are defined as adiabatic slip walls. During the simulations, autoignition occurs within the mixing layer and the structure of flame evolves to steady state. All the results present in this study are obtained from the steady-state solutions.

In this study, 2D steady planar lifted flames are simulated using the in-house solver [37, 38], which is developed based on the open-source CFD framework OpenFOAM. In this solver, the finite volume method is used to solve the fully compressible conservation equations for multi-component reactive flows. Cantera [39] is incorporated for the calculation of reaction rates and transport coefficients. This code was used in recent studies on premixed flames [40–42]. More details on numerical schemes and code validation can be found in references [37, 38]. In all simulations, the thermal and transport properties depend on the temperature and the composition of the mixture. The mixture-averaged model is used for mass diffusion, and the Soret effects are not considered here.

3. Three-stage ignition of DME

In this section, the ignition chemistry of DME is outlined first to explain the three-stage ignition behaviour during the 0D homogenous ignition process, which is shown in Figure 2. Specifically, the transient evolution of temperature, T , and heat release rate, Q , during the 0D homogenous ignition process of fuel lean ($Z \approx 0.4Z_{\text{st}}$) and fuel rich ($Z \approx 2Z_{\text{st}}$) mixtures within the mixing layer of $T_O = 700 \text{ K}$ are plotted in Figure 2. The mass fractions of OH, RO_2 (i.e. $\text{CH}_3\text{OCH}_2\text{O}_2$), H_2O_2 , CO and CO_2 are also plotted. It is seen that for fuel lean case with $Z \approx 0.4Z_{\text{st}}$, three temporally distinct Q peaks are observed, each occurring with a local increase in both T and OH profiles. These three peaks correspond to the instants when the first-, second- and third-stage (main) ignition occurs. Therefore, the ignition delay time is defined accordingly, which are denoted as τ_1 , τ_2 and τ , respectively. Species profiles also show unique features for these three distinct ignition stages. During the first-stage ignition, the low-temperature species RO_2 rises to a maximum value at the end of τ_1 , indicating the importance of LTC in the first-stage ignition. The second-stage ignition is associated with a rapid consumption of the intermediate species, H_2O_2 , which is a feature of ITC. The third-stage ignition is characterised by the slow CO to CO_2 conversion, which is a highly exothermic reaction in the high-temperature oxidation pathway. Besides, it is seen that during the whole ignition process, the first- and second-stage ignition dominates the heat release, indicating the importance of low- and intermediate-temperature chemistries at fuel lean conditions. For the fuel rich case of $Z \approx 2Z_{\text{st}}$, a two-stage ignition is observed wherein LTC is followed by ITC. To qualitatively differentiate the dominant chemistry of each sub-stage ignition, a detailed chemical pathway analysis is performed in Supplementary document and the key reactions for each ignition stage are identified below in Table 1.

Figure 3 shows the ignition delay times over Z -space for 0D homogenous ignition process of the premixtures within the mixing layer for hot air at $T_O = 700, 900$ and 1300 K . It should be noted that a similar study focusing on the LTC and HTC was conducted by Krisman et al. (see Figure 1 in Ref. [8]) using the same setup. Unlike the work of Krisman et al. [8], Figure 3 aims to highlight the role of ITC. It is seen that the three-stage

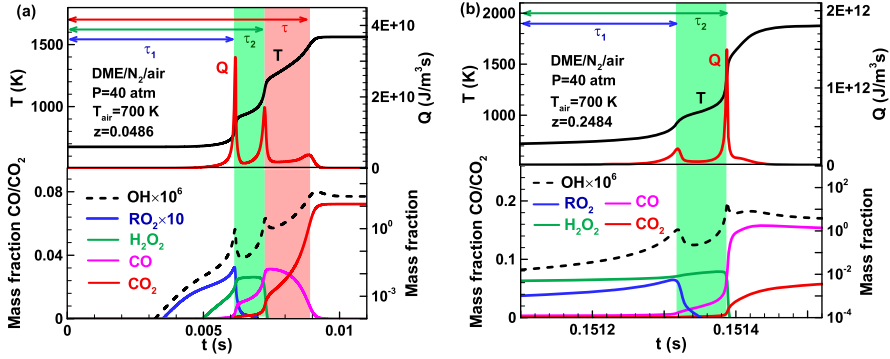


Figure 2. The 0D homogenous ignition process for DME/N₂/air mixture with (a) $Z \approx 0.4Z_{st}$ and (b) $Z \approx 2Z_{st}$ at $T_O = 700$ K and $P = 40$ atm, in which $Z_{st} = 0.1235$ (colour online).

Table 1. Key reactions for heat release and OH production during the low-, intermediate-, and high-temperature ignition stages of DME/N₂/air mixture.

Low-temperature	Intermediate temperature	High temperature
L1: $\text{CH}_3\text{OCH}_3 + \text{OH} = \text{CH}_3\text{OCH}_2 + \text{H}_2\text{O}$	I1: $\text{CH}_2\text{O} + \text{OH} = \text{HCO} + \text{H}_2\text{O}$	H1: $\text{H} + \text{O}_2 = \text{OH} + \text{O}$
L2: $\text{CH}_3\text{OCH}_2 + \text{O}_2 = \text{CH}_3\text{OCH}_2\text{O}_2$	I2: $\text{HCO} + \text{O}_2 = \text{CO} + \text{HO}_2$	H2: $\text{O} + \text{H}_2\text{O} = \text{OH} + \text{OH}$
L3: $\text{CH}_3\text{OCH}_2\text{O}_2 = \text{CH}_2\text{OCH}_2\text{O}_2\text{H}$	I3: $\text{HO}_2 + \text{HO}_2 = \text{H}_2\text{O}_2 + \text{O}_2$	H3: $\text{CO} + \text{OH} = \text{CO}_2 + \text{H}$
L4: $\text{CH}_2\text{OCH}_2\text{O}_2\text{H} + \text{O}_2 = \text{O}_2\text{CH}_2\text{OCH}_2\text{O}_2\text{H}$	I4: $\text{H}_2\text{O}_2(+\text{M}) = \text{OH} + \text{OH}(+\text{M})$	H4: $\text{H} + \text{O}_2(+\text{M}) = \text{HO}_2(+\text{M})$
L5: $\text{O}_2\text{CH}_2\text{OCH}_2\text{O}_2\text{H} = \text{HO}_2\text{CH}_2\text{OCHO} + \text{OH}$	I5: $\text{H}_2\text{O}_2 + \text{OH} = \text{HO}_2 + \text{H}_2\text{O}$	H5: $\text{HO}_2 + \text{OH} = \text{H}_2\text{O} + \text{O}_2$
L6: $\text{HO}_2\text{CH}_2\text{OCHO} = \text{OCH}_2\text{OCHO} + \text{OH}$	I6: $\text{HO}_2 + \text{OH} = \text{H}_2\text{O} + \text{O}_2$	
L7: $\text{CH}_2\text{OCH}_2\text{O}_2\text{H} = \text{OH} + 2\text{CH}_2\text{O}$	I7: $\text{CH}_3 + \text{HO}_2 = \text{CH}_3\text{O} + \text{OH}$	

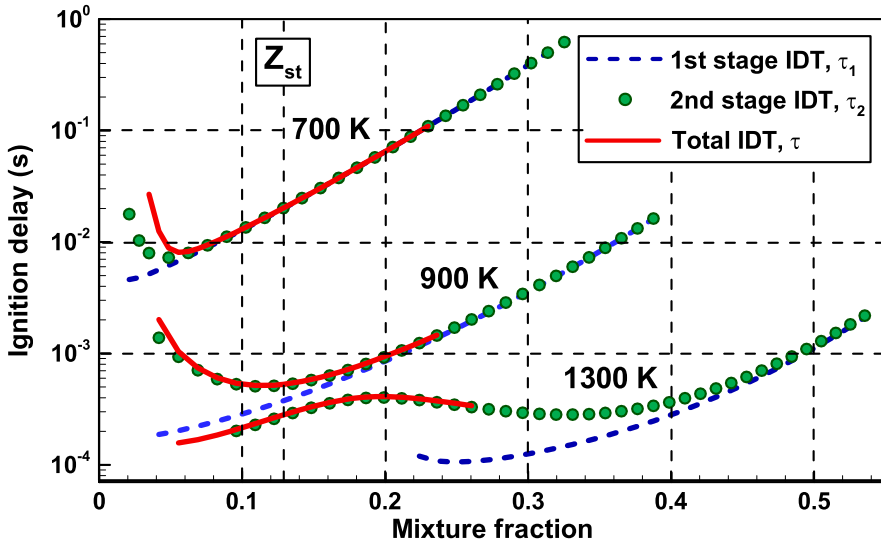


Figure 3. 0D homogenous ignition delay times for LTC (τ_1 , dashed lines), ITC (τ_2 , circles) and HTC (τ , solid lines) over Z -space for various T_O (colour online).

ignition behaviour exists for a wide spectrum of oxidiser temperature from $T_O = 700$ K to 1300 K. At $T_O = 700$ K, three-stage ignition is observed in hot, fuel lean regions. The separate ignition stages gradually collapse in ignition delay time as Z increases. In very rich regions, the HTC vanishes, and a two-stage ignition is observed. This is because on fuel rich side, the deficient reactant O_2 has been fully consumed before high-temperature chemistry starts. As T_O increases to 900 K, the three-stage ignition regime narrows and shifts towards the fuel rich side. However, ITC is found to be close to HTC. When T_O is further increased to $T_O = 1300$ K, two-stage ignition involving temporally close ITC and HTC is observed in high temperature regions, while another two-stage ignition is observed at cold, fuel rich side manifesting sequential LTC and ITC ignitions. The three-stage ignition regime only exists in a narrowed region and thus plays a minor role. Besides, for all the T_O considered, the HTC is replaced by ITC at fuel rich side (e.g. $Z > 0.24$). This indicates that ITC plays an important role in the relatively cold, fuel rich regions. It is noted that here the hot air temperature $T_O = 1300$ K is too high to be representative for diesel engine relevant conditions. This initial temperature is discussed since the case with $T_O = 1300$ K and $\delta = 1000 \mu\text{m}$ can exhibit a unique hexbrachial structure in a 1D diffusion layer as will be shown later, which is of fundamental interest.

It is well-known that DME chemistry contains some peculiarities and uncertainties, especially in the low- and intermediate-temperature regimes [43]. In order to verify the generality of the multi-stage behaviour, besides the mechanism developed by Zhao et al. [23], the DME mechanism recently developed by Wang et al. [43] is also used to calculate ignition delay times for LTC, ITC and HTC. The newly-developed mechanism by Wang et al. [43] has been examined against species concentrations in DME oxidation from low to intermediate temperatures as well as shock tube ignition delay times. It shows satisfactory performance in reproducing the respective literature data. As shown in Supplementary document, the same three-stage ignition behaviour as Figure 3 is obtained with the mechanism by Wang et al. [43]. However, it should be noted that during the development of the low-temperature chemical model, most validation data is limited to those from homogeneous systems. Therefore, the uncertainty in the transport of LTC or ITC related species could also affect the numerical results. In [44], the ignition and extinction of non-premixed DME/air cool flames at elevated pressures were experimentally and computationally investigated in the counterflow. It was found that while the computational results predicted by Zhao et al. model [23] were able to capture the experimental observation of ignition and extinction, as well as the increasing trend of ignition and extinction temperatures with increasing strain rate, quantitative disagreement was observed. Therefore, it is expected that the qualitative findings from this work are reasonable and are independent of the choice of chemical mechanisms, while discrepancy could exist in the quantitative properties, e.g. the ignition delay time.

4. Non-premixed ignition in a 1D diffusion layer

In this section, we study the non-premixed ignition behaviour in a 1D diffusion layer. First, a reference case with $T_O = 1300$ K and $\delta = 1000 \mu\text{m}$ is presented to illustrate the basic ignition process and reaction fronts propagation dynamics in Section 4.1. Then the effects of initial oxidiser temperature and diffusion layer thickness on the non-premixed ignition and the reaction front propagation are discussed in Sections 4.2 and 4.3. Finally, a schematic of reaction front trajectory structures is summarised in Section 4.4.

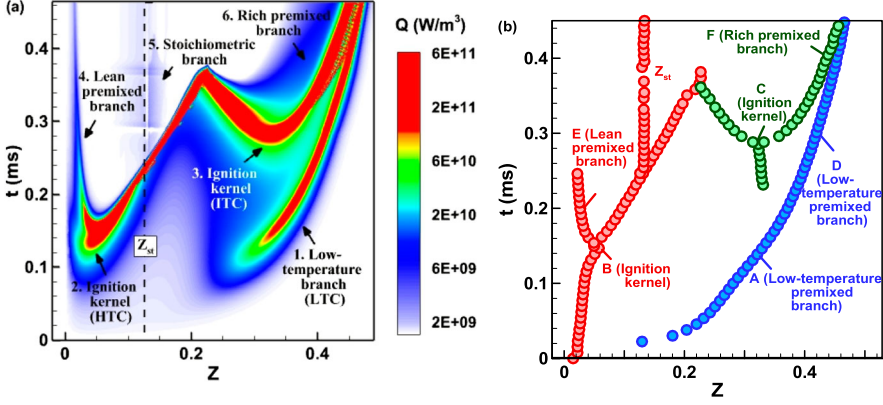


Figure 4. (a) Contour of heat release rate and (b) evolution of the reaction front for $T_O = 1300$ K and $\delta = 1000 \mu\text{m}$ (colour online).

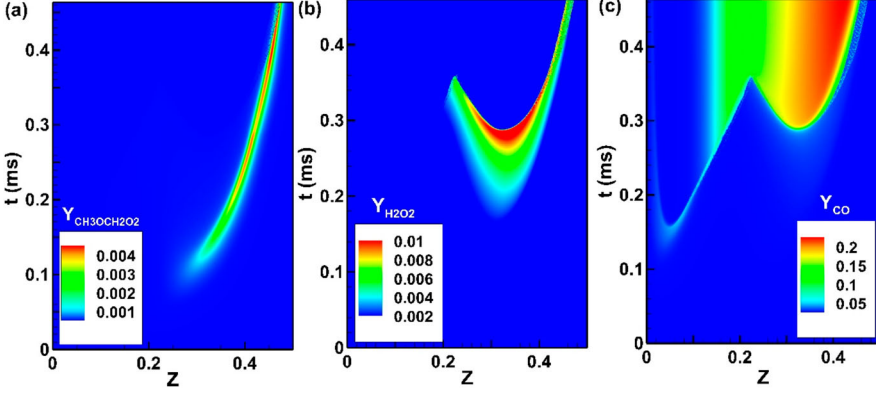


Figure 5. Contours of (a) $\text{CH}_3\text{OCH}_2\text{O}_2$, (b) H_2O_2 , and (c) CO mass fractions for $T_O = 1300$ K and $\delta = 1000 \mu\text{m}$ (colour online).

4.1. Characteristics of the non-premixed ignition process in a diffusion layer

To demonstrate the autoignition process, the contour of heat release rate Q over Z - t space is shown in Figure 4(a). The contours of key species, $Y_{\text{CH}_3\text{OCH}_2\text{O}_2}$, $Y_{\text{H}_2\text{O}_2}$ and Y_{CO} are provided in Figure 5 for reference. It is observed that autoignition first initiates from fuel rich ($Z = 0.33$) and low temperature side at around $t = 140 \mu\text{s}$ (i.e. $\tau_{1\text{st}ig,1D} = 140 \mu\text{s}$). On the other side, another hot spot is formed at $Z = 0.04$ at around $t = 150 \mu\text{s}$ (i.e. $\tau_{2\text{nd}ig,1D} = 150 \mu\text{s}$). Two reaction fronts are created and quickly expand outwardly. It is noticed that the fuel leaner branch of the low temperature ignition gradually vanishes when it propagates to the high temperature region. Therefore, at $t = 1.5\tau_{2\text{nd}ig,1D}$, only three reaction fronts are observed: two formed by high temperature ignition (i.e. ignition occurs at $Z = 0.04$) and one caused by low temperature ignition (i.e. ignition occurs at $Z = 0.33$). Then, a third-stage ignition occurs at $Z = 0.34$ and two new reaction fronts are formed at $t = 285 \mu\text{s}$ (i.e. $\tau_{3\text{rd}ig,1D} = 285 \mu\text{s}$). The new fuel leaner branch then propagates to the high temperature side and finally merges with the high temperature branch at $t = 1.2\tau_{3\text{rd}ig,1D}$. Overall, the reaction front trajectory exhibits a hexbrachial structure, which consists of two

fuel lean premixed branches originated from the high temperature ignition kernel (No. 2 in Figure 4(a)), one low temperature branch (No. 1) and two fuel rich premixed branches initialised by the third ignition kernel (No. 3). Besides, there is also a weak non-premixed branch (No. 5) stabilising at the stoichiometric mixture fraction Z_{st} , which stands for a typical diffusion flame. Compared to the other branches, the flame locating at Z_{st} has a relatively low level of heat release.

To further understand the ignition behaviours described in Figure 4(a), the dominant chemistry and the propagation mechanism of each reaction front are investigated. For better explanation, we track the reaction front and show the evolution of reaction front over mixture fraction space in Figure 4(b). Here, the reaction front is numerically identified as the location of the local maximum O_2 consumption rate, $\dot{\omega}_{O_2, max}$. This definition can track the locations of local heat release peak and local maxima of the temperature gradient [32]. According to the key species contours in Figure 5, the reaction fronts driven by LTC, ITC and HTC are coloured by blue, green, and red, respectively. It is observed that the hexbrachial structure consists of a main HTC driven tribrachial branch, a LTC driven low temperature branch and two ITC driven premixed rich branches. The LTC branch is featured by a local peak in temporal $CH_3OCH_2O_2$ profile. ITC branches are characterised by the consumption of H_2O_2 and formation of CO and HTC branches are associated with the CO to CO_2 conversion. These results indicate that the intermediate temperature chemistry plays an important role at the low temperature and fuel rich side. The ITC branch corresponds to an incomplete combustion process and special attention should be paid to the CO formation and exhaust gas treatment. The dominant chemistry of each reaction front is further examined by chemical pathway analysis, which is shown in Section 3 of the Supplementary document.

Then, we investigate the propagation mode of the reaction front by examining the contribution of chemical reaction term and diffusion term in the governing equations of species. For a deflagration wave, the flame propagation is dominated by the balance between molecular transport and chemical reaction. However, for a spontaneous ignition front, the chemical reaction term is significantly larger than the diffusion term and thereby the front propagation is driven by sequential autoignition (or the gradient of ignition delay [45]). Here, we consider the transport equation for the k -th species:

$$\frac{D}{Dt}(\rho Y_k) = \frac{\partial}{\partial x} \left(\rho D_k \frac{\partial Y_k}{\partial x} \right) + \rho \dot{\omega}_k \quad (5)$$

where Y_k , D_k and $\dot{\omega}_k$ denote the mass fraction, mass diffusivity and reaction rate of the k -th species, respectively. The terms on the right-hand side represent the diffusion and reaction contribution to the reaction front propagation, which is referred to as D and R later, respectively.

The transport budget analysis is performed for $CH_3OCH_2O_2$, H_2O_2 and OH. These species are selected since they are typical markers for LTC [46, 47], ITC [18] and HTC [8], respectively. Figure 6 shows the distribution of diffusion (D) and reaction (R) components, along with the heat release rate Q for points A-F marked in Figure 4(b). For points A-C where the reaction fronts are initialised, the propagation is mainly driven by autoignition. At a later stage, a transition from autoignition-driven to diffusion-driven is observed for the reaction fronts at points D-F, as indicated by an increase in the magnitude of D . It is also seen for point F that the chemical and diffusion terms are well balanced in magnitude, featuring a typical diffusion-driven flame. Therefore, the reaction front at point D-F

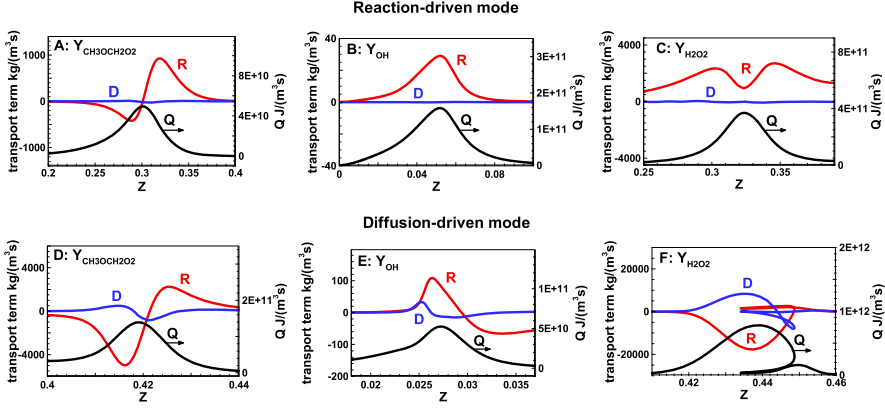


Figure 6. Local transport budget analysis for the reaction fronts in 1D non-premixed ignition process with $T_O = 1300$ K and $\delta = 1000$ μm . The sub-figures show distributions of heat release rate (Q , black lines), two parts of transport terms (R , reaction term, red lines; D , diffusion term, blue lines) in the diffusion layer. These sub-figures correspond to the points A-F marked in the reaction front evolution in Figure 4(b) (colour online).

is identified as a deflagration flame and it propagates in a diffusion-driven mode. It should also be noted that the surrounding premixture at D-F is highly auto-ignitive by which deflagration reaction front can be greatly enhanced. In this study, the conservation equations were solved in physical space and the mixture fraction was defined based on local elements. Therefore, molecular diffusion of radicals will sometimes result in the definition of multi-valued mixture fractions possibly due to differential diffusion (e.g. point F). This behaviour is only caused by the definition of mixture fraction and would not change any physics of the problem. The above results indicate that at an early stage, the reaction front is initialised from autoignition and then propagates as a sequential autoignition front. The growing reaction front induces larger thermal and compositional gradient. As the molecular transport begins to play an essential role, the reaction front develops into a autoignition-assisted deflagration wave. This transition behaviour is observed for LTC, ITC and HTC reaction fronts, and thus is general regardless of the dominant chemistry.

4.2. Effects of hot air temperature

In this sub-section, the hot air temperature is varied to examine the thermochemical effect on the 1D non-premixed ignition. As a comparison to the previous discussion on the case of $T_O = 1300$ K, the reaction front propagation structures at $T_O = 1100$ and 700 K are studied, and the results are shown in Figures 7 and 8.

According to the heat release rate contour for $T_O = 1100$ K shown in Figure 7(a), the reaction front trajectory exhibits a tetrabrachial flame structure, including a conventional tribrachial structure preceded by an additional fuel rich branch initiating from the rich, low-temperature side. To further understand the underlying mechanisms governing each reaction front, similar computational analysis in sub-section 4.1 is conducted and shown in Figure 7(b), where the reaction front is coloured according to the undergoing key chemistry. It is shown that an ITC kernel initiates ($t = 0.3$ ms) in fuel rich mixtures which is partially reacted by the previous LTC front. The ITC kernel leads to the subsequent HTC ignition, which develops into two oppositely moving branches: one propagating towards

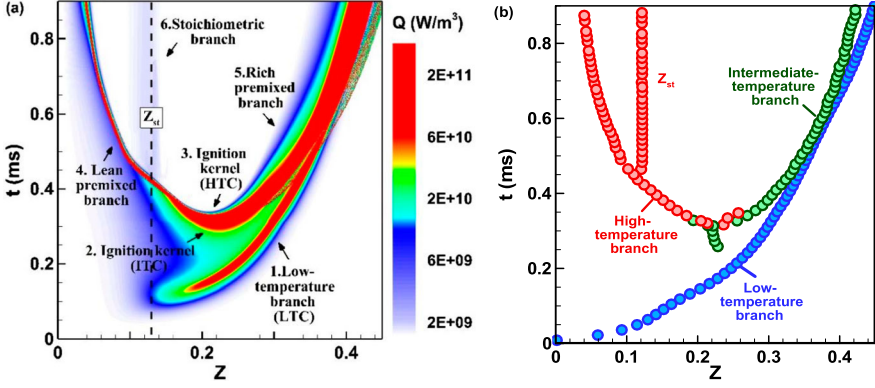


Figure 7. (a) Contour of heat release rate and (b) evolution of the reaction front for $T_O = 1100$ K and $\delta = 1000 \mu\text{m}$ (colour online).

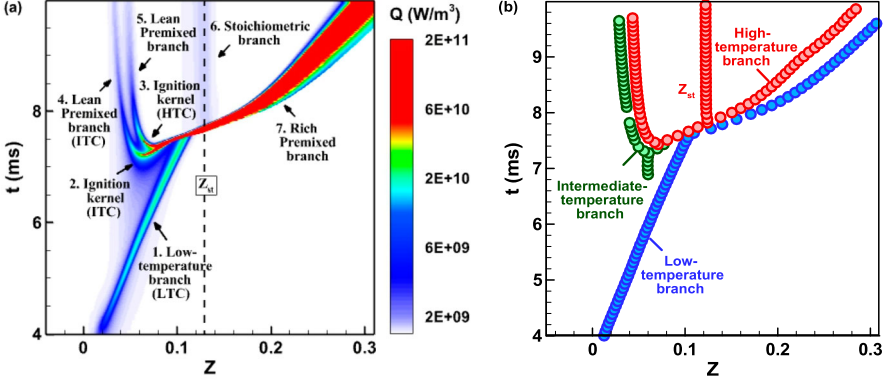


Figure 8. (a) Contour of heat release rate and (b) evolution of the reaction front for $T_O = 700$ K and $\delta = 1000 \mu\text{m}$ (colour online).

the fuel lean side, taking over the leading ITC, then further splitting into a stoichiometric and a fuel lean branch; the other one towards the fuel rich side, gradually weakening and replaced by the rich ITC front. Compared to the case of $T_O = 1300$ K, where various merging and splitting events are observed for the HTC and ITC fronts, less reaction front interactions are observed for $T_O = 1100$ K, and the overall ignition process shows stronger dependence on HTC front as it propagates towards stoichiometry. For both $T_O = 1100$ and 1300 K, the fuel mixture with a high equivalence ratio is consumed by the ITC front following a heading LTC front, indicating that the intermediate temperature chemistry plays an important role in burning out the very rich fuel mixtures in real engines.

As the hot air temperature further decreases to $T_O = 700$ K, there exists significant differences in the structures of reaction front, compared to $T_O = 1100/1300$ K. First, two separate ITC and HTC fronts are observed on the fuel lean side after HTC starts, which is different from the single HTC front as observed in the cases of $T_O = 1100/1300$ K, leading to an overall pentabrachial structure. Second, the initial LTC branch initiates in fuel lean regions, leading to initially fuel lean ITC and HTC ignition kernels. The fuel rich mixtures are consumed by two consecutive LTC/HTC fronts, instead of LTC/ITC fronts as observed

in cases with higher oxidiser temperature. This is because for cases with high oxidiser temperatures (i.e. $T_O = 1300$ and 1100 K), the ITC ignition kernels are located on the fuel rich side and HTC can be easily suppressed by lack of oxygen. However, for $T_O = 700$ K, the initial ITC and HTC kernel are located on the fuel lean side and the right two branches are propagating towards the stoichiometric mixture fraction. During the propagation process, molecular mixing effects enhance the propagation of HTC front such that it takes over the ITC front.

4.3. Effects of diffusion layer thickness

In this sub-section, the analysis is further extended to consider the effect of varying mixing layer thickness on the 1D non-premixed ignition. Figure 9 shows the contour of Q over Z - t space for different T_O and δ , along with the Z - τ plots of 0D homogenous ignition for comparison. The ordinate is normalised by the shortest ignition delay time for ITC and HTC in 0D homogenous ignition process, $\tau_{0D,mr}$, as indicated by the 0D results and Z is normalised by the stoichiometric mixture fraction, Z_{st} .

The first column of Figure 9 corresponds to the cases of $\delta = 1000 \mu\text{m}$, of which the spatial flame structures are discussed in previous contexts for low levels of molecular diffusion effects. Overall, for both cases with $T_O = 1100$ K and $T_O = 1300$ K, the propagation of each reaction front can be well predicted by 0D homogenous ignition. According to previous transport budget analysis results, with a relatively low level of molecular diffusion, the reaction fronts are mainly driven by sequential auto-ignition at an early stage. The reaction front propagates as a sequential autoignition front, which can be accurately predicted by local 0D autoignition. With the accumulation of diffusion effect, the reaction front develops into a deflagration wave, enhanced by the surrounding auto-ignitive premixtures. Therefore, small discrepancy is observed between the upper half of the 1D and 0D plots. The discrepancy is expected to increase with the ratio between the time scales for ignition and molecular diffusion, which is characterised by the inverse of Damkohler (Da) number. In order to distinguish the effects of molecular diffusion and convective transport in the following discussion, the Damkohler number here is defined as $Da_{Diff} = \tau_{Diff}/\tau_{ig,0D}$, in which $\tau_{ig,0D}$ is the delay time of 0D homogenous ignition, and τ_{Diff} is the characteristic diffusion time. We have $\tau_{Diff} = 1/\chi_{st}$, where χ_{st} is the scalar dissipation rate at the stoichiometric mixture fraction (Figure 10), which is defined as $\chi_{st} = (2D(dZ/dx)^2)_{st}$. Here, D is the mass-averaged diffusion coefficient. Therefore, the discrepancy is expected to increase during the reaction front propagation (i.e. when $\tau_{ig,0D}$ increases). With the decrease of oxidiser temperature, the mixture reactivity becomes lower. At $T_O = 700$ K, the characteristic ignition time $\tau_{ig,0D}$ becomes one order larger than that at $T_O = 1100$ and 1300 K. Therefore, Da_{Diff} becomes smaller and molecular diffusion effect becomes more pronounced for $T_O = 700$ K (larger discrepancy is observed between the 1D and 0D plots in Figure 9(c)).

Then the effect of molecular diffusion on the non-premixed ignition is discussed by decreasing δ to 100 and $10 \mu\text{m}$, as shown in the second and third column respectively in Figure 9. For $T_O = 1300$ K, the onset of LTC ignition shows marginal dependence on δ , while the initiation of main-stage combustion at the fuel lean side is significantly delayed by the decreasing δ due to the stronger heat loss induced by increasing thermal gradient. For $\delta = 100$ and $10 \mu\text{m}$, the characteristic diffusion time decreases ($\tau_{Diff} = 1/\chi_{st} \sim 10^{-2}$ 1/s at $\delta = 100 \mu\text{m}$ and $\tau_{Diff} = 1/\chi_{st} \sim 10^{-4}$ 1/s at $\delta = 10 \mu\text{m}$) and thereby the ratio between the time scales for molecular diffusion and ignition, $Da_{Diff} = \tau_{Diff}/\tau_{ig,0D}$ becomes smaller.

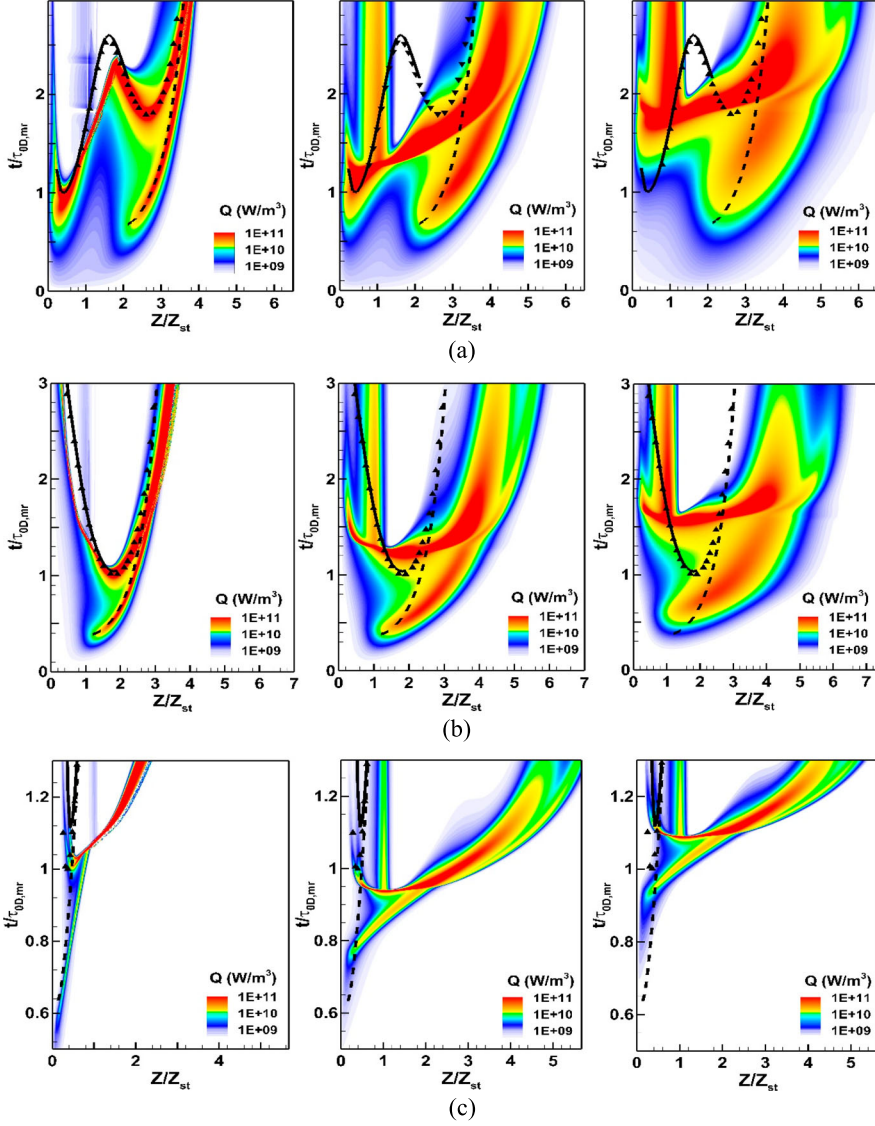


Figure 9. Contours of heat release rate over Z - t space for (a) $T_O = 1300$ K, (b) $T_O = 1100$ K, (c) $T_O = 700$ K with $\delta = 1000, 100, 10 \mu\text{m}$ from left to right. The first-, second-, third-stage ignition delay in 0D cases are shown in each sub-figure using dashed lines, solid triangles, and solid lines, respectively (colour online).

Therefore, the transition of the reaction front from a sequential ignition front to a deflagration flame is expedited. As a result, larger discrepancy is observed between 1D and 0D results as δ decreases. Besides, it is also noticed that the heat release rate of the diffusion flame increases with the decreasing δ , which implies that the diffusion flame is enhanced by the strong molecular transport and the overall oxidation process shows stronger dependence on non-premixed counterpart.

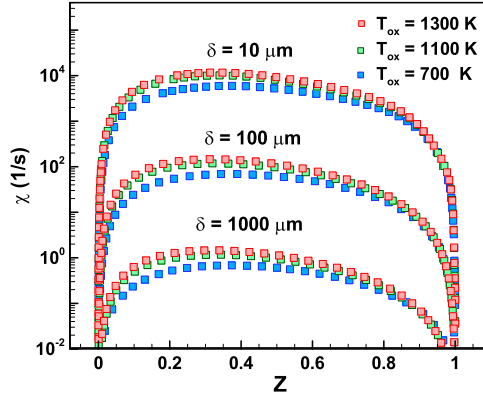


Figure 10. Initial profiles of dissipation rate within the mixing layer for $T_O = 700, 1100, 1300$ K with $\delta = 1000, 100, 10 \mu\text{m}$ (colour online).

As T_O decreases to 1100 K, the main-stage ignition occurs at fuel rich side and is gradually delayed by decreasing δ . One difference is that the LTC is more delayed compared to the 0D results in the presence of strong molecular diffusion ($\delta = 10 \mu\text{m}$). This is because the mixture reactivity is lower in $T_O = 1100$ K, corresponding to a longer characteristic ignition delay time $\tau_{ig,0D}$ and rendering more dependence on molecular diffusion.

As T_O continues to decrease to 700 K, the LTC ignition shows more dependence on δ : decreasing δ delays the LTC initiation but enhances its transition into a deflagration flame. It is also found that the main-stage ignition is first promoted ($\delta = 100 \mu\text{m}$) and then inhibited ($\delta = 10 \mu\text{m}$) with the decreasing δ . This is arguably caused by the fact that at low temperature, the temperature of the ignition spot is not as high as that at high temperature, which induces a lower thermal gradient. As δ decreases, fuel molecules can be more easily transported into the ignition kernel due to the larger compositional gradient, which prevails over the inhibitive effects caused by the heat loss due to the larger thermal gradient, and thus promotes the ignition. When the diffusion layer thickness further decreases to $\delta = 10 \mu\text{m}$, the effect of heat losses becomes dominant again and thus delays the ignition. The non-monotonic behaviour is caused by the competing effects between the fuel transfer into the ignition kernel and heat transfer out of the ignition kernel.

Although the decrease in diffusion layer thickness delays the ignition process for $T_O = 700$ K and $T_O = 1100$ K, it does not vary the basic thermal structures for these two cases. As shown in Figure 9, the reaction front trajectories remain in a tetrabrachial and pentabrachial branch for $T_O = 1100$ K and $T_O = 700$ K. However, for $T_O = 1300$ K, a structure transition from hexbrachial ($\delta = 1000$ and $100 \mu\text{m}$) branch to tetrabrachial ($\delta = 10 \mu\text{m}$) structure is observed. According to the transport budget analysis in the Supplementary document, this phenomenon is caused by the fact that the high temperature branch propagation overtakes the ITC ignition. Therefore, the two reaction fronts caused by ITC ignition kernel are undermined and the overall reaction front trajectory translates into a tetrabrachial structure. Despite it, it is found that ITC still plays an important role when the reaction front enters the intermediate temperature regime. It should be emphasised that the importance of ITC effect cannot be solely indicated by the structure of reaction front trajectory. The only way to evaluate the importance of ITC effect is to perform chemical pathway analysis and identify the dominant chemistry for each reaction front.

In summary, the ignition delay times and thermal structures of the reaction front trajectories in 1D non-premixed ignition mainly depend on the competing effects between autoignition and molecular transport. When the molecular effect is not important (i.e. Da_{Diff} is large), the reaction front propagates in sequential autoignition mode which is basically determined by local autoignition characteristics of the premixture within the diffusion layer. When decreasing the hot oxidiser temperature (increasing $\tau_{ig,0D}$) or decreasing the diffusion layer thickness (decreasing τ_{Diff}), the molecular diffusion becomes essential, which delays or promotes the ignition and translates the sequential auto-ignition fronts into diffusion-driven deflagration flames.

4.4. Schematic of reaction front trajectory structures

The above sub-sections investigate the effects of chemical kinetics and molecular diffusion on the structure of the reaction front trajectory during the 1D non-premixed ignition process. In this context, a regime diagram for different reaction front trajectory structures is proposed and shown in Figure 11.

Qualitatively, when the mixing level is not high ($\chi \sim 10^0$ 1/s), increasing the oxidiser temperature while keeping the constant scalar dissipation rate, the trajectory structure transits from a pentabrachial branch (Regime I) to a tetrabrachial branch (Regime II), then to a hexabrachial branch (Regime III). With each structure including a leading LTC branch and a classical HTC tetrabrachial branch, an ITC reaction front stands on fuel lean side at low oxidiser temperature ($T_O = 700$ K), suppressed at intermediate temperature ($T_O = 900$ and 1100 K), and two ITC reaction fronts are initiated from a separated ignition kernel on fuel rich side at high oxidiser temperature ($T_O = 1300$ and 1500 K).

Similarly, if the mixing level increases at fixed hot oxidiser temperature, the trajectory structure does not significantly vary at low oxidiser temperature ($T_O = 700$ – 1100 K). At high oxidiser temperature ($T_O = 1300$ – 1500 K), transition from a hexabrachial structure (Regime III) to a tetrabrachial structure (Regime II) is achieved by moving vertically across the regime diagram, which has been discussed in sub-section 4.3.

It is noted that a limited number of 1D simulations are conducted to illustrate the structure regime diagram. Therefore, it is difficult to quantify the boundaries between the regimes and only a qualitative trend is presented here.

5. Non-premixed combustion in counterflow and coflow

In the above 1D diffusion layer, convection is induced by thermal expansion and there is no forced convection parallel or normal to the mixture fraction gradient. In this section, the effect of forced convective transport will be discussed by considering non-premixed combustion in 1D counterflow and 2D coflow (as shown in Figure 1b,c). In the literature, the effect of strain rate in 1D counterflow and the effect of inlet velocity in 2D coflow have been widely discussed [9, 13, 48]. To avoid repetitive discussion, the emphasis of this section is placed on demonstrating the importance of newly discovered ITC effect in the thermochemical-diffusive-convective system. To this end, $T_O = 1300$ K is selected as the exemplary case. At $T_O = 1300$ K and $\delta = 1000 \mu\text{m}$, two additional branches are caused by ITC, which offers a good chance to visualise the ITC effects.

Figure 12 compares the response of reaction front/flame structure to varying convective transport in different flow configurations at $T_O = 1300$ K with $\chi \sim 10^0$ 1/s. The heat release rate contours are plotted in mixture fraction-time (Z - t) space for 1D transient counterflow

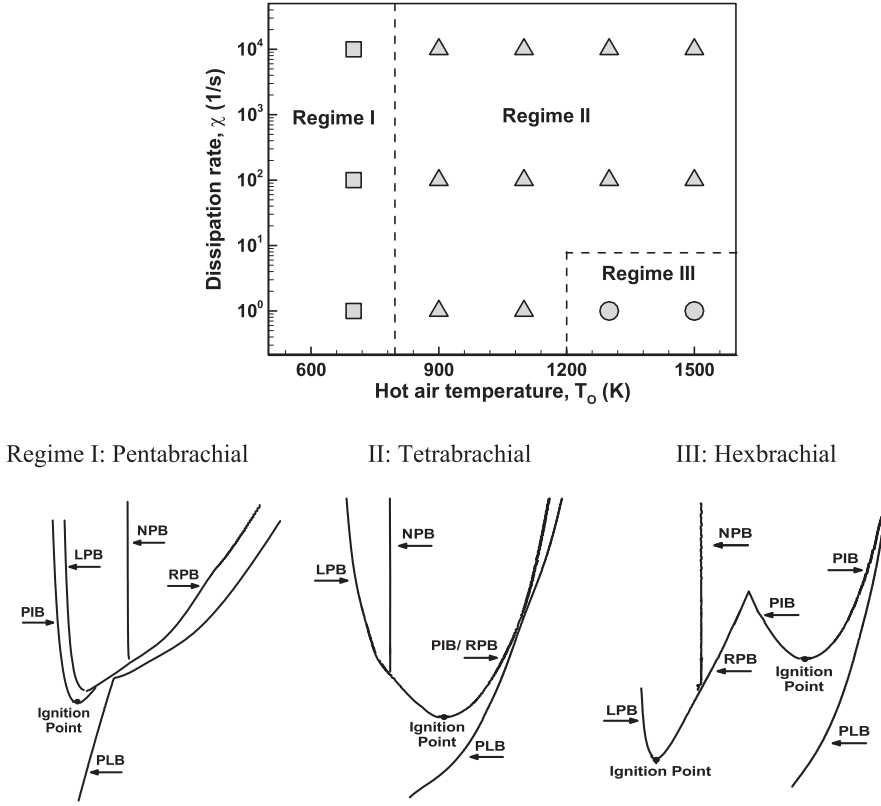


Figure 11. Schematic of the structures of reaction front trajectory predicted by 1D simulations. LPB, NPB and RPB denote lean premixed branch, non-premixed branch, and rich premixed branch for high-temperature chemistry, respectively. PIB denotes premixed branch for intermediate-temperature and PLB denotes premixed branch for LTC. The solid squares, triangles and circles marked in the 2D regime diagram denote the pentabrachial, tetrabrachial and hexbrachial trajectory structures predicted by 1D simulations with varying hot air temperature ($T_0 = 700, 900, 1100, 1300$ and 1500 K) and diffusion layer thickness ($\delta = 10, 100$ and $1000 \mu\text{m}$ with $\chi \sim 10^4, 10^2$ and 10^0 1/s).

autoignition and in mixture fraction-streamwise coordinate (Z - y) space for the 2D lifted flame. By assuming constant velocity along the vertical axis, the unsteady 1D results at different times can be mapped to the ordinate to mimic the flame evolution along the streamwise direction and thereby the 1D reaction front trajectory structures can be compared with 2D lifted flames. As seen from Figure 12, qualitative agreement is observed for the trajectory/flame structures in different configurations, with each contour exhibiting a hexbrachial structure.

In the counterflow configuration, the convective transport is parallel to the temperature and species stratification. Therefore, increasing the fuel and oxidiser stream velocity is expected to vary the mixing level between fuel and oxidiser and modify the local ignition characteristics within the diffusion layer. The effect of forced convection on the transient ignition process can be characterised by $Da_{Conv} = \tau_R / \tau_{ig,0D}$, in which τ_R is the characteristic convection time, and $\tau_{ig,0D}$ is the delay time of 0D homogenous ignition. For a counterflow configuration, τ_R can be defined as $\tau_R = 1/a$, where a is the global strain rate.

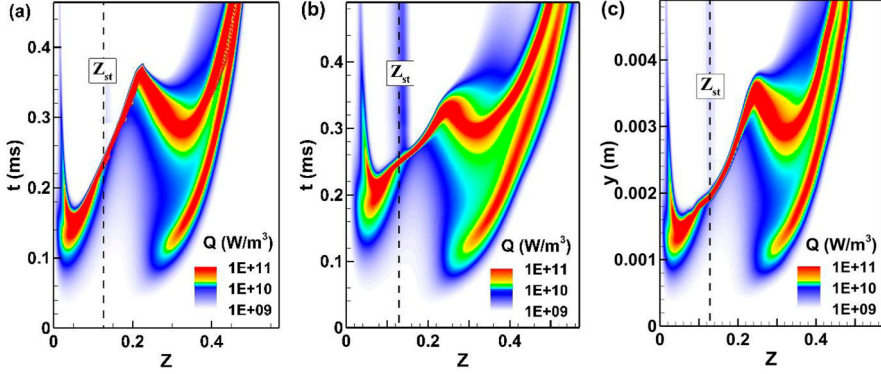


Figure 12. Contours of heat release rate for (a) transient ignition in a 1D diffusion layer, (b) transient ignition in a 1D counterflow and (c) a 2D lifted flame at $T_O = 1300$ K and $\chi \sim 10^0$ 1/s (colour online).

When $T_O = 1300$ K and $\chi \sim 10^0$ 1/s, the strain rate of the flow field is $a = 310$ 1/s. Under such condition, the characteristic ignition delay time ($\tau_{ig,0D} \sim 10^{-4}$ s) is about two orders of magnitude smaller than the characteristic convection time ($\tau_R \sim 10^{-2}$ s). Therefore, the reaction front trajectory is mainly dominated by autoignition and can be well predicted by 1D diffusion layer results at $\delta = 1000$ μ m. Besides, in a 1D diffusion layer, the dissipation rate profile always decays during the transient ignition process, while in the counterflow configuration it is maintained at a fixed level. Therefore, as shown in Figure 12, the heat release rate of the diffusion branch is observed to be the highest in the counterflow configuration among all three cases, indicating that the molecular diffusion is greatly enhanced by forced convection. This enhancing effect is expected to be more pronounced at low oxidiser temperatures, where the time scale of ignition is comparable to that of dissipation rate decay.

On the other hand, in the coflow configuration the convective transport is in the normal direction of the mixture fraction gradient. Previous studies [13, 14] have shown that for an autoignitive system, the thermal structure of 2D lifted flames depends on the stabilisation mechanism, which is influenced by inlet velocity. When the inlet velocity is below a threshold value, the lifted flame is attached to the burner. When the inlet velocity is higher than the threshold value, the flame is stabilised by a kinematic balance between flame speed and incoming flow. Further increasing the inlet velocity, the contribution of autoignition to flame stabilisation would continue to increase. When the inlet velocity is high enough, flame stabilisation mechanism will transit to autoignition stabilisation and only the transport processes parallel to the mixture fraction gradient are important. The effect of inlet velocity on the flame stabilised mechanism can also be characterised by $Da_{Conv} = \tau_R / \tau_{ig,0D}$, which is defined as the ratio between fluid residence time and autoignition delay time. Here, $\tau_R = L / V_{in}$, where L is the lifted height of the flame (from jet exit to flame base) and V_{in} is the inlet velocity. For a sufficient long residence time (i.e. $Da_{Conv} \sim 1$), autoignition occurs in a distributed region and the lifted flame is mainly stabilised by autoignition. A shorter residence time with $Da_{Conv} < 1$ indicates that the autoignition occurs over a smaller region of space, leading to an increased importance of molecular diffusion. When $T_O = 1300$ K and $\chi \sim 10^0$ 1/s, τ_R is in the same order of $\tau_{ig,0D}$ and hence $Da_{Conv} \sim O(1)$. In this context, the lifted flame is mainly stabilised by autoignition and

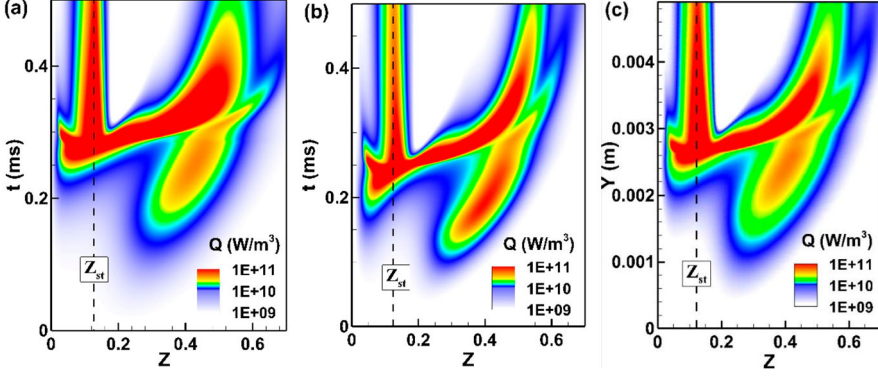


Figure 13. Contours of heat release rate for (a) transient ignition in a 1D diffusion layer, (b) transient ignition in 1D counterflow and (c) 2D lifted flame for $T_O = 1300$ K and $\chi \sim 10^4$ 1/s (colour online).

the thermal structure is controlled by the chemical kinetics and molecular diffusion parallel to the mixture fraction gradient. Therefore, in Figure 12 the flame structure can be qualitatively characterised by 1D diffusion layer results. It is noted that in the coflow configuration, the streamwise convection can also modify the transverse mixing. Therefore, the fuel and oxidiser downstream are expected to be better mixed. However, in the present simulations, high uniform velocities of 10 m/s for both streams are specified at the inlet, which minimises this effect.

As the molecular diffusion effect further increases, the predicted 1D reaction front trajectory translates from a hexbrachial structure (Regime III) to a tetrabrachial structure (Regime II). In counterflow configuration, when the flow strain rate is increased from 310 1/s to 886 1/s, the thickness of the initial diffusion layer decreases from 1000 μm to 10 μm (the dissipation rate increases from $\chi \sim 10^0$ to $\chi \sim 10^4$ 1/s). The Da_{Com} now is in the order of 10^{-1} , which implies that the reaction front trajectory is now more affected by higher mixing level induced by forced convection. Therefore, as shown in Figure 13, the reaction front trajectory can be predicted by 1D diffusion layer with a small thickness (i.e. $\delta = 10 \mu\text{m}$). In 2D coflow configuration, the fluid residence time τ_R is still in the same order of $\tau_{ig,0D}$ in the current case and thereby 2D lifted flames are stabilised by autoignition. Therefore, the current 1D diffusion layer simulation can also qualitatively characterise the overall flame structure in the 2D coflow configuration even for a high dissipation rate case.

The consistent hexbrachial and tetrabrachial structures of the three configurations shown in Figures 12 and 13 indicate that transverse diffusion across the mixing layer is important in producing the complex multibrachial flame structures. Besides, ITC still plays an important role when forced convection is present.

6. Discussion

The above sections have investigated the effects of chemical kinetic, molecular diffusion and convective transport on the thermal and chemical structures of the transient non-premixed autoignition/flames, while the discussion on the convective transport effect is limited. For the completeness, we combine the results from the current study with the

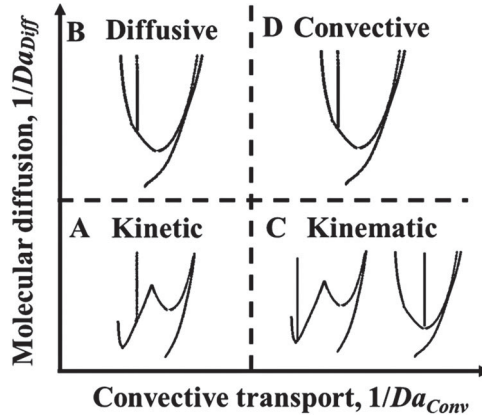


Figure 14. A qualitative regime diagram for the thermal structure of non-premixed combustion at $T_O = 1300$ K, which is classified using two variables: $Da_{Diff} = \tau_{Diff}/\tau_{ig,0D}$ measuring the effect of molecular diffusion, and $Da_{Conv} = \tau_R/\tau_{ig,0D}$ measuring the effect of convective transport.

findings reported by Deng et al. [13] to structure a complete regime diagram which includes all the underlying mechanisms (i.e. chemical kinetics, molecular diffusion and convective transport) that can affect the structure of reaction front and/or flame structures during the non-premixed combustion. A regime diagram for $T_O = 1300$ K is shown in Figure 14 as an example.

Qualitatively, when the molecular diffusion and convective effects are negligible in regime A, i.e. both $1/Da_{Diff}$ and $1/Da_{Conv}$ are small, the thermal structure is basically determined by the autoignition chemistry, which can be characterised by 0D simulations shown in Figure 3. When the molecular diffusion is above certain threshold level (i.e. large $1/Da_{Diff}$ and small $1/Da_{Conv}$ in regime B), the thermal structure is controlled by both chemical kinetics and molecular diffusion, which can be predicted by the 1D diffusion layer regime diagram shown in Figure 11. These two regimes construct a fundamental understanding of the basic ignition and flame regimes in non-premixed combustion. When forced convection is present, the effect of convective transport plays a different role in counterflow and coflow. In the counterflow configuration, the molecular diffusion effect correlates strongly with the convective transport. In this context, the convective transport mainly influences the thermal structure by varying the initial dissipation rate profile (i.e. τ_{Diff} and thereby Da_{Diff}) within the diffusion layer, which is characterised by regimes A and D in the diagram. When $1/Da_{Diff}$ and $1/Da_{Conv}$ are both small (i.e. in regime A), the non-premixed ignition in counterflow is dominated by autoignition chemistry, which can be characterised by 0D simulations results. When $1/Da_{Diff}$ and $1/Da_{Conv}$ are both large (i.e. in regime D), the non-premixed ignition in counterflow is a thermochemical-diffusive system, which can be predicted by the 1D diffusion layer regime diagram. In the coflow configuration, the inlet flow is in the direction normal to the species gradient and thereby the effects of convective transport and scalar dissipation rate can vary independently. Therefore, the lifted flame could be stabilised in any regime in the diagram (i.e. regimes A, B, C, D). When the inlet fluid has a long residence time (i.e. small $1/Da_{Conv}$, regimes A and B), the flame is mainly stabilised by autoignition. The thermal structure is controlled by chemical kinetics and transverse molecular diffusion, which can be predicted by the 0D autoignition and 1D diffusion layer results. When the flame is stabilised by a kinematic

balance between flame speed and incoming flow velocity or even becomes attached to the burner (i.e. large $1/Da_{Conv}$, regimes C and D), the thermal structure is unpredictable. For example, the triple point and the HTC ignition location may appear at approximately the same location (see the structures in regime C). Besides, less branches may be observed for the lifted flame and the main branch of the lifted flame appears as a classical triple flame [13, 14]. This indicates that when treating transient coupling between chemical reactions and mixing, great attention is required, especially when the chemistry is slow compared to mixing (i.e. low relevant Da numbers).

The new regime diagram constructed in this study is a further extension to Deng et al.'s work [9, 13]. As shown in Figure 14, regimes A and C in the diagram include the findings from Deng et al. [9, 13], which show that decreasing the inlet velocity would change the lifted flame stabilisation mechanism from kinetic stabilisation to kinematic stabilisation and even burner stabilisation. Apart from it, the influence of transverse molecular diffusion and the effect of forced convection parallel to the mixture fraction gradient on the non-premixed combustion are also included in the new regime diagram. These effects are characterised by regimes A and B and regimes A and D in Figure 14, respectively.

7. Conclusions

In this work, a systematic analysis is performed to elucidate the individual role of chemical kinetic, molecular diffusion and convective transport in the non-premixed combustion of DME by hot air under engine-relevant conditions. First, 0D homogeneous ignition of the DME/air premixtures is investigated to understand the role of chemical kinetics in the non-premixed autoignition. Apart from the two-stage ignition of DME which typically involves LTC and HTC, the importance of ITC in non-premixed combustion is further identified. It is found that the three-stage ignition behaviour can occur over a wide range of mixture compositions with different hot oxidiser temperatures. Furthermore, relevant species distributions are analyzed to identify the key chemistry associated with each ignition stage. It is found that $\text{CH}_3\text{OCH}_2\text{O}_2$, H_2O_2 , CO and CO_2 can be used as good markers to characterise low-, intermediate-, high-temperature autoignition processes, respectively. Then, 1D diffusion layer simulations are performed under different thermochemical conditions and molecular mixing levels to investigate the effects of chemical kinetics and molecular diffusion. It is found that multiple reaction fronts arise during the three-stage ignition, resulting in a complex multibrachial structure. ITC plays an important role in the non-premixed ignition, especially when burning the rich fuel at intermediate temperature regions, which has often received limited attention in previous studies. Transport budget analysis is conducted and shows that the reaction front initiates from local autoignition near the most reactive regions and then develops into either a sequential autoignition front or a diffusion-driven deflagration flame. Increasing molecular diffusion generally delays the initiation of reaction fronts but enhances the transition into the diffusion-driven flame mode. A 2D regime diagram is proposed to describe the reaction front trajectory structure based on the varying hot oxidiser temperature and scalar dissipation rate. It is seen that when molecular mixing is at a low level, the trajectory structure is basically determined by autoignition characteristics. There is a thermal structure transition from a pentabrachial to tetrabrachial then to hexabrachial structure as T_O increases from 700 to 1500 K. Increasing molecular diffusion reduces the number of reaction front branches since the reaction fronts originating from autoignition are taken over by the diffusion-driven flames. Finally, 1D

counterflow and 2D coflow simulations are conducted to understand the autoignition process of DME in the hot air environment with the presence of both molecular diffusion and forced convective transport. It is found that the 1D diffusion layer simulations can qualitatively predict the multibrachial flame structures obtained from 1D counterflow and 2D lifted flame simulations at certain conditions. The reasonably good agreement indicates the importance of transverse diffusion across the mixing layer in producing the complex multibrachial flame structures. Combining the results obtained in this work with the findings reported in the literature, a complete regime diagram is proposed to qualitatively separate the effects of chemical kinetics, molecular diffusion, convective transport, and kinematics on the non-premixed combustion of DME under engine-relevant conditions.

In present study, it is demonstrated that ITC shows an important role in the fuel rich, intermediate temperature regions over a wide range of thermochemical conditions, mixing levels and flow conditions. So far, the three-stage ignition behaviour of DME under engine-relevant conditions has not been observed in experiments. Therefore, in future work, it would be interesting to validate such phenomenon in experiments. Furthermore, in practical engines, turbulent flames always experience a large fluctuation in local temperature, dissipation rate and flow velocity. Therefore, the ITC effect investigated in this study could have important implications for turbulent non-premixed combustion under engine-relevant conditions, especially for fuel efficiency and pollutant formation. In literature, there are many studies on single- and two-stage ignition in a turbulent mixing layer (e.g. [1, 49–51]). In future works, it would also be interesting to consider the influence of turbulence on the three-stage ignition.

Disclosure statement

No potential conflict of interest was reported by the author(s).

Funding

This work is jointly supported by the National Natural Science Foundation of China (Nos. 52176096 and 51861135309) and the German Research Foundation (DFG, no. 411275182).

Supplemental data

Supplemental data for this article can be accessed here <https://doi.org/10.1080/13647830.2023.2261423>.

ORCID

Christian Hasse  <http://orcid.org/0000-0001-9333-0911>

References

- [1] A. Krisman, E.R. Hawkes, M. Talei, A. Bhagatwala and J.H. Chen, *A direct numerical simulation of cool-flame affected autoignition in diesel engine-relevant conditions*. Proc. Combust. Inst. 36 (2017), pp. 3567–3575.
- [2] R. Knikkerr, A. Dauplain, B. Cuenot and T. Poinsot, *Comparison of computational methodologies for ignition of diffusion layers*. Combust. Sci. Technol. 175 (2003), pp. 1783–1806.
- [3] C.K. Law, *Combustion Physics*, Cambridge University Press, Cambridge, 2006.
- [4] S. Deng, D. Han and C. Law, *Ignition and extinction of strained nonpremixed cool flames at elevated pressures*. Combust. Flame 176 (2017), pp. 143–150.

- [5] X.L. Zheng, T.F. Lu, C.K. Law, C.K. Westbrook and H.J. Curran, *Experimental and computational study of nonpremixed ignition of dimethyl ether in counterflow*. Proc. Combust. Inst. 30 (2005), pp. 1101–1109.
- [6] J. Buckmaster, *Edge-flames*. Prog. Energy Combust. Sci. 28 (2002), pp. 435–475.
- [7] S.H. Chung, *Stabilization, propagation and instability of tribrachial triple flames*. Proc. Combust. Inst. 31 (2007), pp. 877–892.
- [8] A. Krisman, E.R. Hawkes, M. Talei, A. Bhagatwala and J.H. Chen, *Polybrachial structures in dimethyl ether edge-flames at negative temperature coefficient conditions*. Proc. Combust. Inst. 35 (2015), pp. 999–1006.
- [9] S. Deng, P. Zhao, M.E. Mueller and C.K. Law, *Autoignition-affected stabilization of laminar nonpremixed DME/air coflow flames*. Combust. Flame 162 (2015), pp. 3437–3445.
- [10] K.S. Jung, S.O. Kim, T. Lu, S.H. Chung, B.J. Lee and C.S. Yoo, *Differential diffusion effect on the stabilization characteristics of autoignited laminar lifted methane/hydrogen jet flames in heated coflow air*. Combust. Flame 198 (2018), pp. 305–319.
- [11] B.C. Choi, K.N. Kim and S.H. Chung, *Autoignited laminar lifted flames of propane in coflow jets with tribrachial edge and mild combustion*. Combust. Flame 156 (2009), pp. 396–404.
- [12] K. Van, K.S. Jung, C.S. Yoo, S. Oh, B.J. Lee, M.S. Cha, J. Park and S.H. Chung, *Decreasing liftoff height behavior in diluted laminar lifted methane jet flames*. Proc. Combust. Inst. 37 (2019), pp. 2005–2012.
- [13] S. Deng, P. Zhao, M.E. Mueller and C.K. Law, *Stabilization of laminar nonpremixed DME/air coflow flames at elevated temperatures and pressures*. Combust. Flame 162 (2015), pp. 4471–4478.
- [14] D.K. Dalakoti, K. Alex, S. Bruno, W. Armin, H. Wang, M.S. Day, J.B. Bell and E.R. Hawkes, *Structure and propagation of two-dimensional, partially premixed, laminar flames in diesel engine conditions*. Proc. Combust. Inst. 37 (2019), pp. 1961–1969.
- [15] S.H. Park and C.S. Lee, *Corrigendum to Combustion performance and emission reduction characteristics of automotive DME engine system*. Prog. Energy Combust. Sci. 39 (2013), pp. 147–168.
- [16] Y. Ju, C.B. Reuter, O.R. Yehia, T. Farouk and S.H. Won, *Dynamics of cool flames*. Prog. Energy Combust. Sci. 75 (2019), pp. 100787.
- [17] C.K. Westbrook, *Chemical kinetics of hydrocarbon ignition in practical combustion systems*. Proc. Combust. Inst. 28 (2000), pp. 1563–1577.
- [18] S.M. Sarathy, E. Tingas, E.F. Nasir, A. Detogni, Z. Wang, A. Farooq and H. Im, *Three-stage heat release in n-heptane auto-ignition*. Proc. Combust. Inst. 37 (2019), pp. 485–492.
- [19] H. Oshibe, H. Nakamura, T. Tezuka, S. Hasegawa and K. Maruta, *Stabilized three-stage oxidation of DME/air mixture in a micro flow reactor with a controlled temperature profile*. Combust. Flame 157 (2010), pp. 1572–1580.
- [20] M. Tao, Q. Yang, P. Lynch and P. Zhao, *Auto-ignition and reaction front dynamics in mixtures with temperature and concentration stratification*. Front. Mech. Eng. 6 (2020), pp. 68.
- [21] G. Issayev, S.M. Sarathy and A. Farooq, *Autoignition of diethyl ether and a diethyl ether/ethanol blend*. Fuel 279 (2020), pp. 118553.
- [22] Y. Ju, *Understanding cool flames and warm flames*. Proc. Combust. Inst. 38 (2021), pp. 83–119.
- [23] Z. Zhao, M. Chaos, A. Kazakov and F.L. Dryer, *Thermal decomposition reaction and a comprehensive kinetic model of dimethyl ether*. Int. J. Chem. Kinet. 40 (2008), pp. 1–18.
- [24] A. Bhagatwala, Z. Luo, H. Shen, J.A. Sutton, T. Lu and J.H. Chen, *Numerical and experimental investigation of turbulent DME jet flames*. Proc. Combust. Inst. 35 (2015), pp. 1157–1166.
- [25] R.W. Bilger, *The structure of turbulent nonpremixed flames*. Symp. Combust. 22 (1989), pp. 475–488.
- [26] H. Pitsch and N. Peters, *A consistent flamelet formulation for non-premixed combustion considering differential diffusion effects*. Combust. Flame 114 (1998), pp. 26–40.
- [27] P. Dai and Z. Chen, *Supersonic reaction front propagation initiated by a hot spot in n-heptane/air mixture with multistage ignition*. Combust. Flame 162 (2015), pp. 4183–4193.
- [28] Z. Chen, *Effects of radiation and compression on propagating spherical flames of methane/air mixtures near the lean flammability limit*. Combust. Flame 157 (2010), pp. 2267–2276.
- [29] Z. Chen, M.P. Burke and Y. Ju, *On the critical flame radius and minimum ignition energy for spherical flame initiation*. Int. J. Chem. Kinet. 33 (2011), pp. 1219–1226.

- [30] Y. Wang, W. Han and Z. Chen, *Effects of fuel stratification on ignition kernel development and minimum ignition energy of n-decane/air mixtures*. Proc. Combust. Inst. 37 (2019), pp. 1623–1630.
- [31] M. Faghih, W. Han and Z. Chen, *Effects of Soret diffusion on premixed flame propagation under engine-relevant conditions*. Combust. Flame 194 (2018), pp. 175–179.
- [32] Z. Li, X. Gou and Z. Chen, *Effects of hydrogen addition on non-premixed ignition of iso-octane by hot air in a diffusion layer*. Combust. Flame 199 (2019), pp. 292–300.
- [33] X. Chen, H. Bottler, A. Scholtissek, C. Hasse and Z. Chen, *Effects of stretch-chemistry interaction on chemical pathways for strained and curved hydrogen/air premixed flames*. Combust. Flame 232 (2021), pp. 111532.
- [34] X. Chen, P. Zhao, P. Dai and Z. Chen, *On the prediction of hot spot induced ignition by the Livengood-Wu integral*. Proc. Combust. Inst. 38 (2021), pp. 4709–4716.
- [35] W. Han, Z. Sun, A. Scholtissek and C. Hasse, *Machine learning of ignition delay times under dual-fuel engine conditions*. Fuel 288 (2020), pp. 119650.
- [36] A. Zschuttschke, D. Messig, A. Scholtissek, C. Hasse, Universal Laminar Flame Solver (ULF), https://figshare.com/articles/ULF_code_pdf/5119855, (2017)
- [37] T. Zirwes, F. Zhang, P. Habisreuther, M. Hansinger, H. Bockhorn, M. Pfitzner and D. Trimis, *Quasi-DNS dataset of a piloted flame with inhomogeneous inlet conditions*. Flow Turbul. Combust. 104 (2020), pp. 997–1027.
- [38] T. Zirwes, F. Zhang, J.A. Denev, P. Habisreuther, H. Bockhorn, Automated code generation for maximizing performance of detailed chemistry calculations in OpenFOAM, high performance computing in science and engineering ‘ 172018
- [39] D.G. Goodwin, *Cantera C++ user’s guide*, California Institute of Technology, California, 2002.
- [40] Y. Wang, H. Zhang, T. Zirwes, F. Zhang, H. Bockhorn and Z. Chen, *Ignition of dimethyl ether/air mixtures by hot particles: impact of low temperature chemical reactions*. Proc. Combust. Inst. 38 (2021), pp. 2459–2466.
- [41] T. Zirwes, F. Zhang, P. Habisreuther, M. Hansinger, H. Bockhorn, M. Pfitzner and D. Trimis, *Identification of flame regimes in partially premixed combustion from a quasi-DNS dataset*. Flow Turbul. Combust. 106 (2021), pp. 373–404.
- [42] T. Zirwes, T. Häber, F. Zhang, H. Kosaka, A. Dreizler, M. Steinhausen, C. Hasse, A. Stagni, D. Trimis, R. Suntz and H. Bockhorn, *Numerical study of quenching distances for side-wall quenching using detailed diffusion and chemistry*. Flow Turbul. Combust. 106 (2021), pp. 649–679.
- [43] Z. Wang, X. Zhang, L. Xing, L. Zhang, F. Herrmann, K. Moshhammer, F. Qi and K. Kohse-Hoeinghaus, *Experimental and kinetic modeling study of the low- and intermediate-temperature oxidation of dimethyl ether*. Combust. Flame 162 (2015), pp. 1113–1125.
- [44] S. Deng, D. Han and C.K. Law, *Ignition and extinction of strained nonpremixed cool flames at elevated pressures*. Combust. Flame 176 (2017), pp. 143–150.
- [45] Y.B. Zeldovich, *Regime classification of an exothermic reaction with nonuniform initial conditions*. Combust. Flame 39 (1980), pp. 211–214.
- [46] H. Yamada, K. Suzaki, A. Tezaki and Y. Goto, *Transition from cool flame to thermal flame in compression ignition process*. Combust. Flame 154 (2008), pp. 248–258.
- [47] W. Zhang, M. Faghih, X. Gou and Z. Chen, *Numerical study on the transient evolution of a premixed cool flame*. Combust. Flame 187 (2018), pp. 129–136.
- [48] B. Wang, Z. Li, H.C. Lee, P. Dai and X. Gan, *A computational study on the transient ignition and NTC behavior of non-premixed dimethyl ether/air counterflow under elevated pressure*. Energy Fuels 34 (2020), pp. 6383–6391.
- [49] E. Mastorakos, T.A. Baritaud and T. Poinsot, *Numerical simulations of autoignition in turbulent mixing flows*. Combust. Flame 109 (1997), pp. 198–223.
- [50] R. Hilbert and D. Thevenin, *Autoignition of turbulent non-premixed flames investigated using direct numerical simulations*. Combust. Flame 128 (2002), pp. 22–37.
- [51] T. Jin, K.H. Luo, X. Wang, K. Luo and J. Fan, *Dynamics of triple-flames in ignition of turbulent dual fuel mixture: A direct numerical simulation study*. Proc. Combust. Inst. 37 (2019), pp. 4625–4633.